A CT-Based Radiomics Nomogram To Predict The Biological Activity of Hepatic Alveolar Echinococcosis

Jian Wang
Xinjiang Medical University Affiliated First Hospital
Tieliang Zhang
Xinjiang Medical University Affiliated First Hospital
Yi Jiang
Southern University of Science and Technology
Yafei Zhao
Xinjiang Medical University Affiliated First Hospital
Wenyao Xu
Xinjiang Medical University
Yuwei Xia
Huiying Medical Technology Co Ltd
Wenya Liu (13999202977@163.com)
Xinjiang Medical University Affiliated First Hospital

Research

Keywords: Alveolar echinococcosis, Tomography, X-Ray Computed, PET/CT, Radiomics, nomogram

Posted Date: September 2nd, 2021

DOI: https://doi.org/10.21203/rs.3.rs-812332/v1

Abstract

Background

This study aims to establish a computed tomography (CT) - based radiomics nomogram to predict the biological activity of hepatic alveolar echinococcosis (HAE).

Methods

A total of 174 HAE patients (139 for training, 35 for test) were enrolled whose CT and positron emission tomography-computed tomography (PET/CT) examinations were performed before surgery, and the biological activity was evaluated according to the PET/CT. Radiomic features were extracted from CT images, based on which radiomic scores (Rad-score) were calculated with the least absolute shrinkage and selection operator logistic regression. Three radiomics models (K-Nearest Neighbors, Logical regression, and Multilayer Perceptron), including only radiomic features and a radiomics nomogram, comprised of demographics, clinical indexes, and radiomic features were constructed respectively to predict the biological activity of HAE. The model performance was evaluated by area under curve (AUC), decision curve, and calibration curve.

Results

30 features in total were selected as optimal radiomic features and considered as input to calculate the Rad-score. There were no significant differences in the predictive efficacy between the combined models and the radiomics models from the perspective of the decision curve. The radiomics models was unparalleled, with an AUC of 0.952 (95%CI=0.902~0.981, P<0.0001) and 0.800 (95%CI=0.631~0.916, P<0.0020) in the training and testing cohort, respectively.

Conclusion

The radiomics nomogram model showed great potential in identifying HAE biological activity.

Introduction

Hepatic alveolar echinococcosis (HAE) is caused by the parasitic metacestode Echinococcus multilocularis, which was rare but life-threatening. Most patients are diagnosed at the advanced stage because of the hidden early symptoms of HAE[1] and can barely benefit from the radical operation [2, 3], which leads patients had to complete lifelong pharmacological treatment with benzimidazoles-albendazole (ABZ) or mebendazole (MBZ) [3, 4], and thorough follow-ups. Patients have to suffer from drug side effects [5] and the high cost of treatment [6]. Unfortunately, there is no an effective curative effect evaluation standard for parasiticidal drug targeting metacestode stages of the parasite [7]. 18F fluorodeoxyglucose (18F-FDG) positron emission computed tomography (PET/CT), which is currently considered reliable, has been used for this purpose [8, 9, 10, 11]. Recent studies have shown that the inactivity of PET/CT is the main drug cessation indicator [12, 13]. However, complicated equipments and

high healthcare costs limit its widespread acceptance as routine HAE evaluation. Thus, an economical and practical alternative is still badly needed.

As well known, characteristics have been set up to describe HAE on many imaging modalities such as ultrasound, CT, or MR images.Some feasible results in terms of lesion activity evaluation have been achieved in some studies [14, 15, 16, 17]compared to PET/CT based on morphology and imaging features (calcification and microcysts sign). But it remains challenging for radiologists to find well-validated imaging markers to determine metacestode viability in HAE. The concept of radiomics has attracted increased attention in recent years [18]. In liver diseases, radiomics models have been involved in fibrosis staging, portal hypertension evaluating, and focal lesions qualitative diagnosis [19], and radiomics models constructed by incorporating clinical features of hepatocellular carcinoma (HCC) could improve the predictive ability of microvascular invasion (MVI) and pathological grading efficiency[20, 21, 22].

To our knowledge, no previous studies have built a CT-based radiomics nomogram for HAE. Despite the disadvantage of radiation problem, CT is the most widely used imaging modality for detection in most countries.

This study aims to develop and validate a CT-based radiomics nomogram that would incorporate radiomics signature and clinical factors to evaluate HAE activity.

Materials And Methods

Patients

This retrospective study was approved by our Ethical Committee, and informed consent was waived for the patients. All procedures involving human participants adhered to the tenets of the Declaration of Helsinki.

The initial 248 patients were reviewed from May 2012 to January 2021. The inclusion criteria were as follows: (1) confirmed HAE by surgery or biopsy; (2) high quality of CT scan were available; (3) PET/ CT were available within 15 days before or after CT scan; (4)complete medical records were at hand, including age, sex, height, weight, body mass index (BMI), and PNM stage (P: parasitic mass in the liver, N: involvement of neighboring organs, M: metastasis)[23].Patients were excluded if any of the inclusion criteria was violated as shown in **figure 1**. The patients were randomly divided into a training set and test set at the ratio of 8:2. The training set contains 139 HAE patients, of which 99 were active and 40 were inactive. The test set contains 35 HAE patients, of which 25 were active and 10 were inactive.

CT Image Acquisition

All patients underwent a plain scan and contrast-enhanced imaging with a 64-Detector Row CT Scanner (LightSpeed VCT & Discovery 750, GE Medical Systems, USA) with the same scan protocol. CT images were acquired during a single breath-hold. After routine non-enhanced CT, the contrast-enhanced CT scan

was initiated after an intravenous administration of 1.5 mL/kg of the iodinated contrast material (Uitravist 370, Bayer HealthCare, Germany) at a rate of 3.0-3.5 mL/s via a high-pressure injector (Tennessee XD2003, Ulrich GmbH & Co. KG, Germany). Three phase-enhanced CT scans were performed, including the arterial phase, portal venous phase, and equilibrium phase. The CT protocol was as follows: volume scan, 120 kVp of tube voltage with automatic tube current modulation, 0.5s of rotation time, 64mm×0.625mm of detector collimation, 5mm slice thickness and interval, 0.984 of pitch, 512mm×512mm of a matrix.

Conventional Radiological Characteristics Analysis and Classification

Images were analyzed by two radiologists, both with more than 10 years of experience in diagnosing abdominal diseases. The two radiologists evaluated the images independently over indexes such as signs of microcysts, Graeter classification, and calcification [16]. The calcification analysis was based on Graeter`s research (1: without calcification; 2: feathery calcification; 3: focal calcification; 4: diffuse calcification; 5: mainly calcification, edge calcification, and central calcification). One senior radiologist with 15 years of experience in abdomen images was supposed to decide for inconsistent cases.

18F-FDG-PET/CT imaging protocol and image interpretation

All images were obtained from a Discovery VCT PET/CT (GE Healthcare Bio-Sciences, Pittsburgh, PA, USA) with an 18F-FDG tracer produced by Cyclotron (GE Healthcare Bio-Sciences) that had a radiochemical purity of >95%. Patients were intravenously injected with 18F-FDG (7.4 MBq/kg body weight). All patients were treated with standard 18F-FDG-PET/CT acquisition (PET/CT acquisition was performed 1 h after 18F-FDG injection). The delayed 18F-FDG-PET/CT acquisition was performed 3h after 18F-FDG injection if necessary[11]. The image diagnosis (with a definite “active” or “inactive” label) was made by one experienced radiologists and reviewed by the senior radiologist. The standardized uptake value (SUV) was calculated automatically by semi-quantitative analysis in the workstation. Cases with higher lesion SUV indicates active, lower lesion SUV indicates inactive , compared to that of peripheral liver parenchyma.

Lesion Segmentation and Image preprocessing

The lesion segmentation was performed on the rad cloud platform (version 3.1.0, http://radcloud.cn/, Huiying Medical Technology Co., Ltd, Beijing, China). The volumes of interest (VOIs) were delineated layer by layer along the edge of the lesion in the portal venous phase (the optimal imaging phase for lesion boundary) by one radiologist. All the VOIs were visually confirmed by another senior radiologist. The two radiologists did not know whether the lesions were active when evaluating the imaging. Representative CT images for inactive and active lesions are shown in **Figure 2**.

To improve the stability of radiomic features, the images were pre-processed by standard deviation normalization [μ-3σ, μ + 3σ], and B-spline interpolation sampling to resample all CT images to1.0×1.0×1.0 mm^3 to unify the slice thickness.

Feature extraction and normalization

The quantitative features of VOIs were calculated at radcloud platform, which was in compliance with definitions described by the Image Biomarker Standardisation Initiative (IBSI). The IBSI is an international collaboration developed to help standardize radiomic feature calculation, which has made recommendations concerning feature calculation, standardized feature definition, and nomenclature [24, 25]. A total of 1409 radiomics features were extracted, which included first-order features, shape features, and texture features, which included gray level co-occurrence matrix (GLCM), gray level size zone matrix (GLSZM), gray level run length matrix (GLRLM), neighboring gray-tone difference matrix (NGTDM), and gray level dependence matrix (GLDM). The selected radiomics features of model were in additional file 1 (Table S1).

In feature normalization, Z-score normalization was applied to eliminate the difference in the value scale of the extracted features. The mean value is subtracted from the original feature value and the above results were further divided by the standard deviation.

Features Selection and model construction

To effectively select available features from high dimensional feature sets, the least absolute shrinkage and selection operator (LASSO) logistic regression algorithm was utilized in the training dataset. Rad-score for each patient was calculated by using a linear combination of selected features, each weighted by respective LASSO coefficients. The formula used to calculate Rad-score was in additional file 1 (Formula S1).

Supervised machine learning classifiers including K-Nearest Neighbors (KNN), Logical regression (LR), and Multilayer Perceptron (MLP), were applied to develop radiomics models, training in the training dataset and applied in the test dataset. The areas under the receiver operating characteristic (ROC) curves (AUCs) along with 95% confidence intervals (CIs) were used to assess the predictive efficiency of the model, and the cutoff value was selected according to the Youden index to determine the corresponding sensitivity and specificity.

The radiomics and clinical nomogram construction and evaluation

Furthermore, in order to improve the predictive performance of the current Rad-score-based model, the clinical indicators highly correlated with biological activity were introduced into this predictive model. Univariate analysis was first initiated to select the most highly correlated indicators. A radiomics nomogram was established with both Rad-score and previous selected clinical indicators to predict HAE biological status. Calibration curves and decision curves were delineated to assess the calibration and feasible clinical utility.

Statistical analysis

Software R Version 3.6.3 (https://www.R-project.org/) was used for statistical analysis and models development [25]. For continuous variables, the Kolmogorov-Smirnov test was first used to evaluate normality. Independent sample t-test was utilized for the data with normal distribution and expressed as mean (standard deviation). Otherwise, the data were analyzed by the Mann-Whitney U test and expressed as median [IQR]. Chi-square test and Fisher's exact probability method were used to compare the categorical variables between groups. DeLong's test was used to compare the differences among models. A two-tailed $P < 0.05$ was considered to be statistically significant.

Result

Patients Clinical and Conventional Image Factors

The characteristics of the patients in the training and testing sets were described in **Table 1**. According to PET/CT indexes, P stage, microcysts sign were significantly different ($p < 0.05$) between the active group and inactive group in the training set and test set; calcification was significantly different ($p < 0.05$) in training set only; the gender, age, height, weight, BMI, N stage, and M stage were not significantly different ($p > 0.05$) between the active group and inactive group.

Table 1 Characteristics of the HAE patients in the active group and inactive group

Characteristic	Training Group (n=139)				Testing Group (n=35)			
	Total	Active	Inactive	p-value	Total	Active	Inactive	p-value
Gender				0.953				0.033
Male	62	44	18		18	10	8	
Female	77	55	22		17	15	2	
Age mean (SD), year		40.55 (14.52)	38.71 (12.40)	0.452		38.28 (11.08)	41.60 (16.30)	0.49
Height mean (SD), cm		162.63 (7.87)	163.65 (8.04)	0.491		165.08 (6.20)	161.80(11.06)	0.271
Weight mean (SD), kg		58.95 (12.28)	61.25 (12.51)	0.322		59.72 (9.55)	60.70 (11.02)	0.794
BMI mean (SD)		22.19 (3.69)	22.73 (3.54)	0.431		21.87 (2.99)	23.00 (2.41)	0.299
P stage				<0.001				0.01
P1		0	2			0	1	
P2		11	13			4	4	
P3		37	14			6	3	
P4		51	11			15	2	
N stage				0.727				0.504
N0		65	25			18	6	
N1		34	15			7	4	
M stage				0.055				0.227
M0		57	30			18	5	
M1		42	10			7	5	
microcysts				0.004				0.001
Y		55	12			10	0	
N		44	28			15	10	
calcification				0.007				0.857
1		4	2			1	1	
2		22	2			6	1	
3		52	19			11	7	

4	17	8	7	0	
5	4	7	0	1	

SD, standard deviation.

Radiomics Models Establishment and Validation

The best performance of LASSO regression was built using a penalty parameter -log(α) = 1.58, as the mean square error was minimized resulted in 30 radiomic features from the 1409 image features (**Figure 3**). The radiomic features showed good predictive accuracy among three classifiers (**Table 2**) according to AUC, sensitivity, and specificity (**Figure 4**), with MLP achieved the best.

Table 2 Radiomics models' performance in predicting the biological activity of HAE

Models	Group	AUC (95% CI)	Accuracy	Sensitivity	Specificity	Youden	Cutoff	p-value
KNN	Train	0.827 (0.753–0.885)	0.676	0.566	0.950	0.516	0.889	<0.0001
	Test	0.748 (0.573–0.879)	0.629	0.520	0.900	0.42	0.889	0.0085
LR	Train	0.844 (0.772–0.900)	0.827	0.879	0.700	0.579	0.503	<0.0001
	Test	0.796 (0.626–0.913)	0.800	0.800	0.800	0.6	0.555	0.0024
MLP	Train	0.952 (0.902–0.981)	0.835	0.788	0.950	0.738	0.794	<0.0001
	Test	0.800 (0.631–0.916)	0.800	0.800	0.800	0.6	0.684	0.0020

Nomogram Construction and Validation

In the univariate analysis of the training cohort, the P stage, microcysts sign, and calcification showed significant differences between the active and inactive group. Therefore, a radiomics nomogram model incorporating Rad-score with the clinical indicator was constructed (**figure 5A**). Calibration curves for the radiomics nomogram are shown good consistency between predictive outcome and observation in the training and test sets (**figure 5B, C**). The results of decision curve analysis (DCA) in the training set are shown in **Figure 6.** The DCA showed satisfactory performance for the radiomics nomogram model while

the proposed radiomics model showed a greater advantage. There were no significant differences in the predictive efficacy between the combined models and the single radiomics model.

Graeter Classification for Activity Prediction

The results of Graeter classification in the active group and inactive group are shown in **Table. 3**. The chi-square test results (λ^2=12.205, p=0.0321) show a positive correlation between the Graeter classification and PET/CT result for activity evaluation. Furthermore, KNN, LR, and MLP models were also applied to evaluate the predictive efficiency of Graeter. In the training set, the sensitivity, specificity, accuracy, and AUC (95%CT) of KNN, LR, MLP were 0.949, 0.171, 0.719, 0.561 (0.513~0.682); 0.949, 0.171, 0.719, 0.524 (0.414~ 0.586); 0.378, 0.829, 0.511, 0.637 (0.529~0.696), respectively. In the test set, the sensitivity, specificity, accuracy, and AUC of KNN, LR, MLP were 1.000, 0.000, 0.743, 0.500□0.383~0.727□; 0.038, 1.000, 0.286, 0.457 (0.327~ 0.673); 0.269, 0.889, 0.429, 0.577 (0.423~0.763), respectively (**Figure 7**), indicating bad performance of three Graeter classification based models.

Table 3 The Graeter classification for HAE patients

Graeter	Activity of HAE		
	Active	Inactive	
□	11	2	13(7.5%)
□	75	35	110(63.2%)
□a	33	6	39(22.4%)
□b	4	4	8(4.6%)
□	1	1	2(1.1%)
□	0	2	2(1.1%)
	124(71.3%)	50(28.7%)	174

Discussion

HAE is a fatal parasitic disease mainly popular in the temperate countryside and high-altitude mountainous areas. The untreated 10-year mortality was more than 90% [26, 27]. PET/CT, the preferred imaging modality, showed the response of inflammatory cells around parasitic lesions, thus indirectly reflecting metabolic activity [10, 28]. CT examination was earlier used in HAE evaluation of drug therapy[29], compared with PET/CT, partly because CT equipment is more readily available, especially in these remote pastoral areas. Radiomics based model was not satisfactory compared with clinical indicators based model in predicting the pathological grade or microvascular invasion for HCC [30]. Still, when combined with clinical indicators, the nomogram model becomes better [20]. Therefore, this

research was designed to establish a radiomics nomogram with clinical and traditional imaging features to predict HAE biological status.

In this study, three machine learning algorithms were utilized to build prediction models, namely KNN, LR, and MLP, capturing the linear and nonlinear relationships of data, with AUCs ranging from 0.748 to 0.800 in the testing cohort, with MLP achieved the top results. This may be partly due to the fact that the MLP network models the computational units of multiple layers by imitating signal transmission, and the layers of deep neural architecture overcome the limitation of local minimum optimization [31]. The Greater-MLP model which based on CT morphology classification, with an AUC of 0.58 and 0.64 in the training and testing cohort. Eventually, a combined nomogram model incorporated the radiomics signature and clinical features while no significant differences were detected between the combined model and the radiomics models.

Among clinical markers, the PNM stage indicated the clinical stages derived from the World Health Organization staging system[23]. Our results showed that P stage was related to the AE activity in that with the P stage increased, the nomogram score decreased, implying that a higher the P stage would lead to an inactive lesion. Microcysts sign is one of the most typical image features for HAE. In pathology, the HAE lesions were shown multiple vesicles /microcysts(from 1 mm to 1.1cm in diameter) on gross specimen [2, 32]. On CT scan, the small vesicles were represented by small round low density and most clearly displayed in portal vein phase. Previous studies demonstrated that it is related to HAE activity and our results further confirm it [14].

Calcification is considered as another manifestation of HAE and in most cases, increased calcification would indicate stable progression [23, 33], which is quite similar to Greater's calcification classification [16]. However, Brumpt considered micro calcifications (similar to Greater's feathery calcification) related to activated status. Clinically, microcalcifcations/feathery calcifications come up with macrocalcifications in most cases, thus indicating that the increase in calcification maybe a marker of stable progression. Therefore in the current study, Greater classification was utilized.

There are still some Limitations to this research. Firstly, this is a retrospective study and the included subjects were heterogeneous, including both untreated and chemotherapy-treated patients, which may cause bias for the results; Secondly, in the delineation of ROI, only portal vein phase images were included in this study and features from CT plain scans and CT enhanced arterial phase images were needed to be verified in future; Finally, multicenter research is necessary because there are different characteristics for HAE In different countries and regions[34].

In conclusion, a CT-based radiomics nomogram can evaluate the biological activity of HAE and it is expected to be a more convenient method for follow-up after drug treatment.

Abbreviations

HAE: Hepatic alveolar echinococcosis; PET/CT: computed tomography; Body mass index (BMI): AUC: Area under the curve; ABZ: benzimidazoles-albendazole; HCC: hepatocellular carcinoma; SUV: Standardized uptake value; VOIs:Volumes of interest; IBSI:Standardisation Initiative; GLCM: gray level co-occurrence matrix; GLSZM: gray level size zone matrix; GLRLM: gray level run length matrix; NGTDM: neighboring gray-tone difference matrix; GLDM: gray level dependence matrix; LASSO: least absolute shrinkage and selection operator; KNN: K-Nearest Neighbors; LR: Logical regression: MLP: Multilayer Perceptron; CIs: Confidence intervals; DCA: Decision curve analysis.

Declarations

Acknowledgements

Thanks to all participants in this study.

Authors' contributions

WL, YJ, and JW designed the study. JW, YX, YZ, and TZ performed analyses. JW and YJ wrote the manuscript. JW, YZ, and WX collected data. WL, YJ, and JW contributed to the discussion and manuscript revision. All authors contributed to the article and approved the submitted version.

Funding

This study was supported by the National Natural Science Foundation of China (81974263, 81760331)

Availability of data and materials

The original contributions presented in the study are included in the article/supplementary material. However, the image datasets in the current study are not publicly available due to patient privacy protection, but further inquiries can be directed to the corresponding authors.

Ethics approval and consent to participate

This retrospective study was approved by the Medical Ethics Review Committee of the First Affiliated Hospital of Xinjiang Medical University, and exempted from informed consent.

Consent for publication

Not applicable.

Competing interests

The authors declare that they have no competing interests.

Author details

[1]Department of Imaging Center, The First Affiliated Hospital of Xinjiang Medical University, Li Yu Shan Road, No. 137 Urumqi City 830054, China. [2]Radiology Department, Southern University of Science and Technology Hospital, Shenzhen 518055, China. [3]Huiying Medical Technology Co., Ltd., Room A206, B2, Dongsheng Science and Technology Park, HaiDian District, Beijing City 100192, China.

References

1. Chauchet A, Grenouillet F, Knapp J, Richou C, Delabrousse E, Dentan C, et al. Increased incidence and characteristics of alveolar echinococcosis in patients with immunosuppression-associated conditions. Clin Infect Dis. 2014;59 8:1095–104. doi:10.1093/cid/ciu520.
2. Wen H, Vuitton L, Tuxun T, Li J, Vuitton DA, Zhang W, et al. Echinococcosis: Advances in the 21st Century. Clin Microbiol Rev. 2019;32 2; doi:10.1128/cmr.00075-18.
3. Vuitton DA, Azizi A, Richou C, Vuitton L, Blagosklonov O, Delabrousse E, et al. Current interventional strategy for the treatment of hepatic alveolar echinococcosis. Expert Rev Anti Infect Ther. 2016;14 12:1179–94. doi:10.1080/14787210.2016.1240030.
4. Zavoikin VD, Zelya OP, Tumolskaya NI. The importance of uninterrupted albendazole treatment in patients with unresectable alveolar echinococcosis undergoing liver transplantation. Transpl Infect Dis. 2020;22(4):e13291. doi:10.1111/tid.13291.
5. María AC, Celina EM. Efficacy of albendazole in combination with thymol against Echinococcus multilocularis protoscoleces and metacestodes. Acta Trop. 2014;140:61–7. doi:10.1016/j.actatropica.2014.08.007.
6. Lötsch F, Budke CM, Auer H, Kaczirek K, Waneck F, Lagler H, et al. Evaluation of direct costs associated with alveolar and cystic echinococcosis in Austria. PLoS Negl Trop Dis. 2019;13(1):e0007110. doi:10.1371/journal.pntd.0007110.
7. Gottstein B, Wang J, Blagosklonov O, Grenouillet F, Millon L, Vuitton DA, et al. Echinococcus metacestode: in search of viability markers. Parasite. 2014;21:63. doi:10.1051/parasite/2014063.
8. Reuter S, Schirrmeister H, Kratzer W, Dreweck C, Reske SN, Kern P. Pericystic metabolic activity in alveolar echinococcosis: assessment and follow-up by positron emission tomography. Clin Infect Dis. 1999;29 5:1157–63. doi:10.1086/313438.
9. Stumpe KD, Renner-Schneiter EC, Kuenzle AK, Grimm F, Kadry Z, Clavien PA, et al. F-18-fluorodeoxyglucose (FDG) positron-emission tomography of Echinococcus multilocularis liver lesions: prospective evaluation of its value for diagnosis and follow-up during benzimidazole therapy. Infection. 2007;35(1):11–8. doi:10.1007/s15010-007-6133-9.
10. Reuter S, Gruener B, Buck AK, Blumstein N, Reske SN. Long-term follow-up of metabolic activity in human alveolar echinococcosis using FDG-PET. Nuklearmedizin. 2008;47:4:147–52.
11. Caoduro C, Porot C, Vuitton DA, Bresson-Hadni S, Blagosklonov O. The Role of Delayed F-18-FDG PET Imaging in the Follow-up of Patients with Alveolar Echinococcosis. J Nucl Med. 2013;54:3.

12. Ammann RW, Stumpe K, Felix G, Peter D, Sabine H, Kaja B, et al. Outcome after discontinuing long-term Benzimidazole treatment in 11 patients with non-resectable Alveolar Echinococcosis with negative FDG-PET/CT and anti-EmII/3–10 serology. PLoS Neglected Tropical Diseases. 2015;9:9:e0003964.
13. Husmann L, Muehlematter UJ, Grimm F, Ledergerber B, Messerli M, Kudura K, et al. PET/CT helps to determine treatment duration in patients with resected as well as inoperable alveolar echinococcosis. Parasitol Int. 2021;83:102356. doi:10.1016/j.parint.2021.102356.
14. Azizi A, Blagosklonov O, Lounis A, Berthet L, Vuitton DA, Bresson-Hadni S, et al. Alveolar echinococcosis: correlation between hepatic MRI findings and FDG-PET/CT metabolic activity. Abdom Imaging. 2015;40 1:56–63. doi:10.1007/s00261-014-0183-0.
15. Kodama Y, Fujita N, Shimizu T, Endo H, Nambu T, Sato N, et al. Alveolar echinococcosis: MR findings in the liver. Radiology. 2003;228(1):172–7. doi:10.1148/radiol.2281020323.
16. Graeter T, Kratzer W, Oeztuerk S, Haenle MM, Mason RA, Hillenbrand A, et al. Proposal of a computed tomography classification for hepatic alveolar echinococcosis. World J Gastroenterol. 2016;22 13:3621–31. doi:10.3748/wjg.v22.i13.3621.
17. Brumpt E, Blagosklonov O, Calame P, Bresson-Hadni S, Vuitton DA, Delabrousse E. AE hepatic lesions: correlation between calcifications at CT and FDG-PET/CT metabolic activity. Infection. 2019;47 6:955–60. doi:10.1007/s15010-019-01328-z.
18. Lambin P, Rios-Velazquez E, Leijenaar R, Carvalho S, van Stiphout RG, Granton P, et al. Radiomics: extracting more information from medical images using advanced feature analysis. Eur J Cancer. 2012;48(4):441–6. doi:10.1016/j.ejca.2011.11.036.
19. Park HJ, Park B, Lee SS. Radiomics and Deep Learning: Hepatic Applications. Korean J Radiol. 2020;21 4:387–401. doi:10.3348/kjr.2019.0752.
20. Zhang X, Ruan S, Xiao W, Shao J, Tian W, Liu W, et al. Contrast-enhanced CT radiomics for preoperative evaluation of microvascular invasion in hepatocellular carcinoma: A two-center study. Clin Transl Med. 2020;10(2):e111. doi:10.1002/ctm2.111.
21. Jiang YQ, Cao SE, Cao S, Chen JN, Wang GY, Shi WQ, et al. Preoperative identification of microvascular invasion in hepatocellular carcinoma by XGBoost and deep learning. J Cancer Res Clin Oncol. 2021;147(3):821–33. doi:10.1007/s00432-020-03366-9.
22. Mao B, Zhang L, Ning P, Ding F, Wu F, Lu G, et al. Preoperative prediction for pathological grade of hepatocellular carcinoma via machine learning-based radiomics. Eur Radiol. 2020;30 12:6924–32. doi:10.1007/s00330-020-07056-5.
23. Kern P, Wen H, Sato N, Vuitton DA, Gruener B, Shao Y, et al. WHO classification of alveolar echinococcosis: principles and application. Parasitol Int 2006;55 Suppl:S283-7; doi:10.1016/j.parint.2005.11.041.
24. Zwanenburg A, Leger S, Vallières M, Lck S. Image biomarker standardisation initiative. Radiotherapy & Oncology; 2016.

25. Zwanenburg A, Vallières M, Abdalah MA, Aerts H, Andrearczyk V, Apte A, et al. The Image Biomarker Standardization Initiative: Standardized Quantitative Radiomics for High-Throughput Image-based Phenotyping. Radiology. 2020;295(2):328–38. doi:10.1148/radiol.2020191145.
26. Wilson JF, Rausch RL, McMahon BJ, Schantz PM. Parasiticidal effect of chemotherapy in alveolar hydatid disease: review of experience with mebendazole and albendazole in Alaskan Eskimos. Clin Infect Dis. 1992;15(2):234–49. doi:10.1093/clinids/15.2.234.
27. Weng X, Mu Z, Wei X, Wang X, Zuo Q, Ma S, et al. The effects of dog management on Echinococcus spp. prevalence in villages on the eastern Tibetan Plateau, China. Parasit Vectors 2020;13 1:207; doi:10.1186/s13071-020-04082-6.
28. Porot C, Knapp J, Wang J, Germain S, Camporese D, Seimbille Y, et al. Development of a specific tracer for metabolic imaging of alveolar echinococcosis: A preclinical study. Annu Int Conf IEEE Eng Med Biol Soc. 2014;2014:5587–90. doi:10.1109/embc.2014.6944893.
29. Liu YH, Wang XG, Chen YT, Yao YQ. Computer tomography of liver in alveolar echinococcosis treated with albendazole. Trans R Soc Trop Med Hyg. 1993;87 3:319–21. doi:10.1016/0035-9203(93)90147-i.
30. Huang J, Tian W, Zhang L, Huang Q, Lin S, Ding Y, et al. Preoperative Prediction Power of Imaging Methods for Microvascular Invasion in Hepatocellular Carcinoma: A Systemic Review and Meta-Analysis. Front Oncol. 2020;10:887. doi:10.3389/fonc.2020.00887.
31. Lee JG, Jun S, Cho YW, Lee H, Kim GB, Seo JB, et al. Deep Learning in Medical Imaging: General Overview. Korean J Radiol. 2017;18 4:570–84. doi:10.3348/kjr.2017.18.4.570.
32. Reinehr M, Micheloud C, Grimm F, Kronenberg PA, Grimm J, Beck A, et al. Pathology of Echinococcosis: A Morphologic and Immunohistochemical Study on 138 Specimens With Focus on the Differential Diagnosis Between Cystic and Alveolar Echinococcosis. Am J Surg Pathol. 2020;44 1:43–54. doi:10.1097/pas.0000000000001374.
33. Graeter T, Shi R, Bao HH, Kratzer W, Barth TFE, Hillenbrand A, et al. Follow-up in hepatic alveolar echinococcosis under benzimidazole therapy using computed tomography. Chin Med J (Engl). 2020;133 12:1507–9. doi:10.1097/cm9.0000000000000874.
34. Graeter T, Bao HH, Shi R, Liu WY, Li WX, Jiang Y, et al. Evaluation of intrahepatic manifestation and distant extrahepatic disease in alveolar echinococcosis. World J Gastroenterol. 2020;26 29:4302–15. doi:10.3748/wjg.v26.i29.4302.

Figures

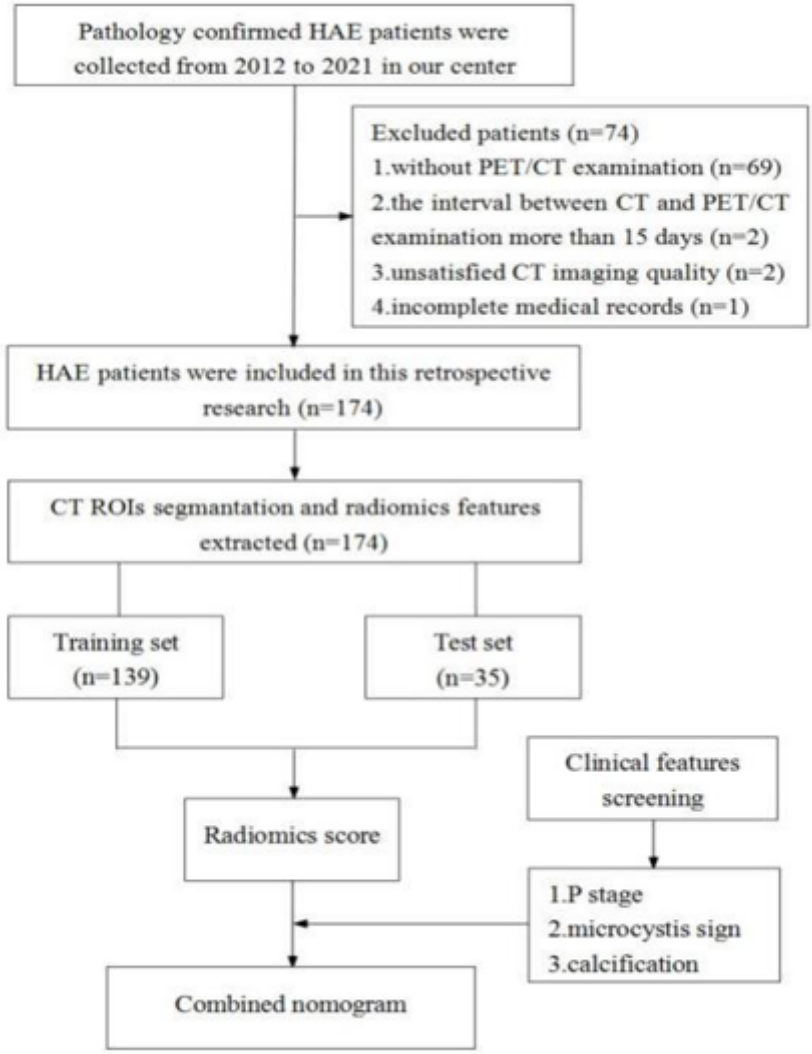

Figure 1

The research work flow

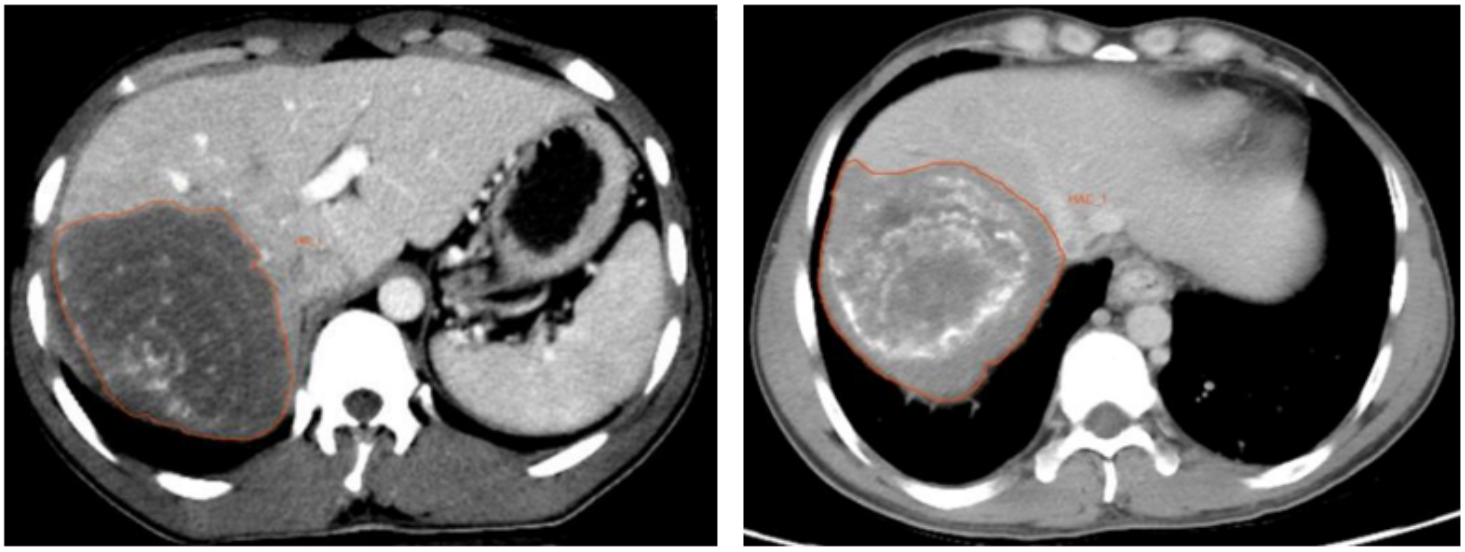

Figure 2

The CT images for inactive and active HAE. A: 26 years old male HAE patient, inactive lesion in the right hepatic lobe, Graeter type; B: 35 years old male HAE patient, active lesion in the right lobe of liver, also Graeter type.

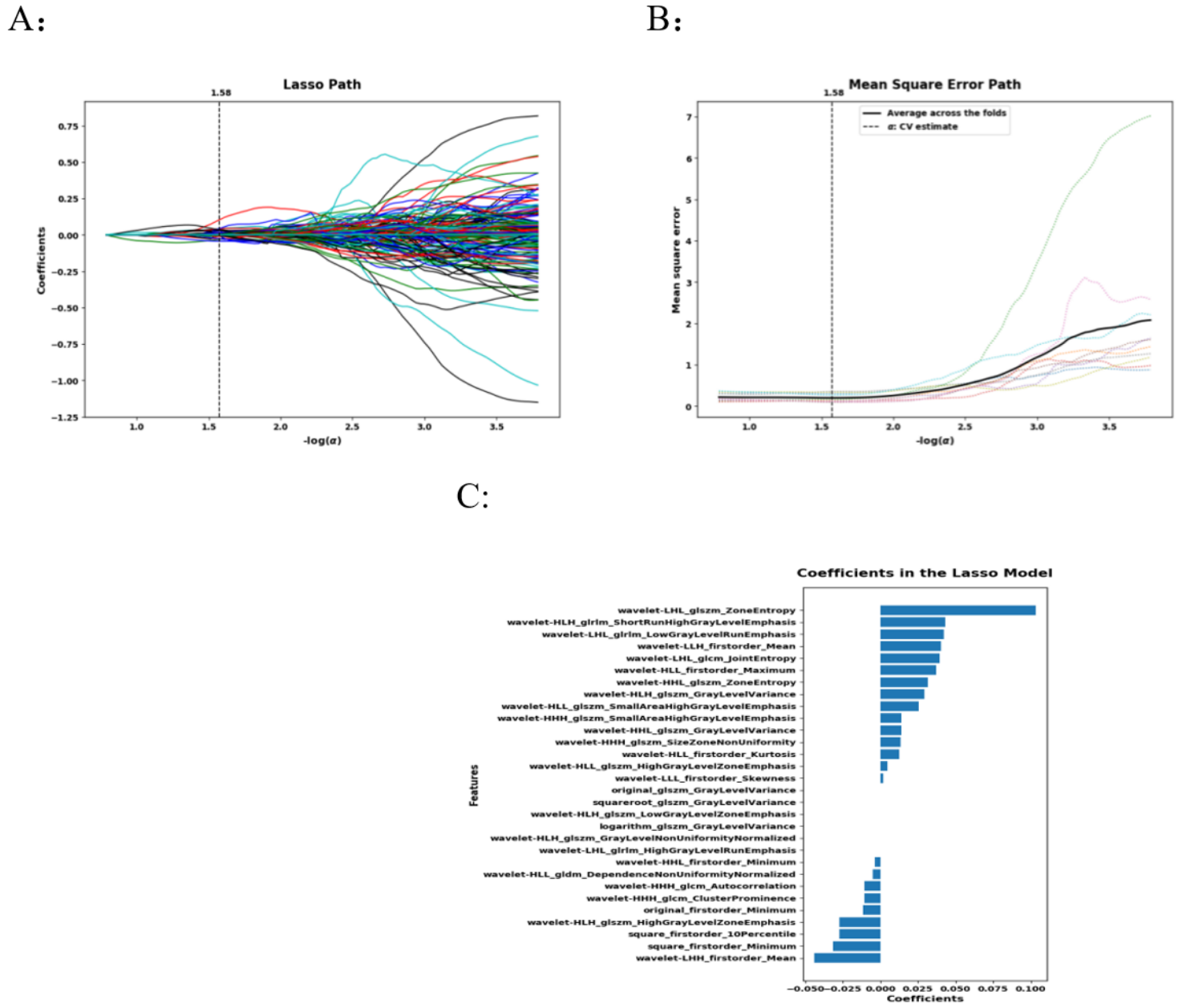

Figure 3

Feature selection for the LASSO regression model on CT images. A. parameter -log(α) selection in the LASSO model. The top value represents the corresponding characteristic number. This study selected the optimal -log(α) value corresponding to the perpendicular line to obtain 30 features with non-zero coefficients. B. Mean Square Error of LASSO coefficients for different features as modulation parameter (-log(α) value) changes. C. Contributions of the 30 selected features to the LASSO model, with their respective coefficient values.

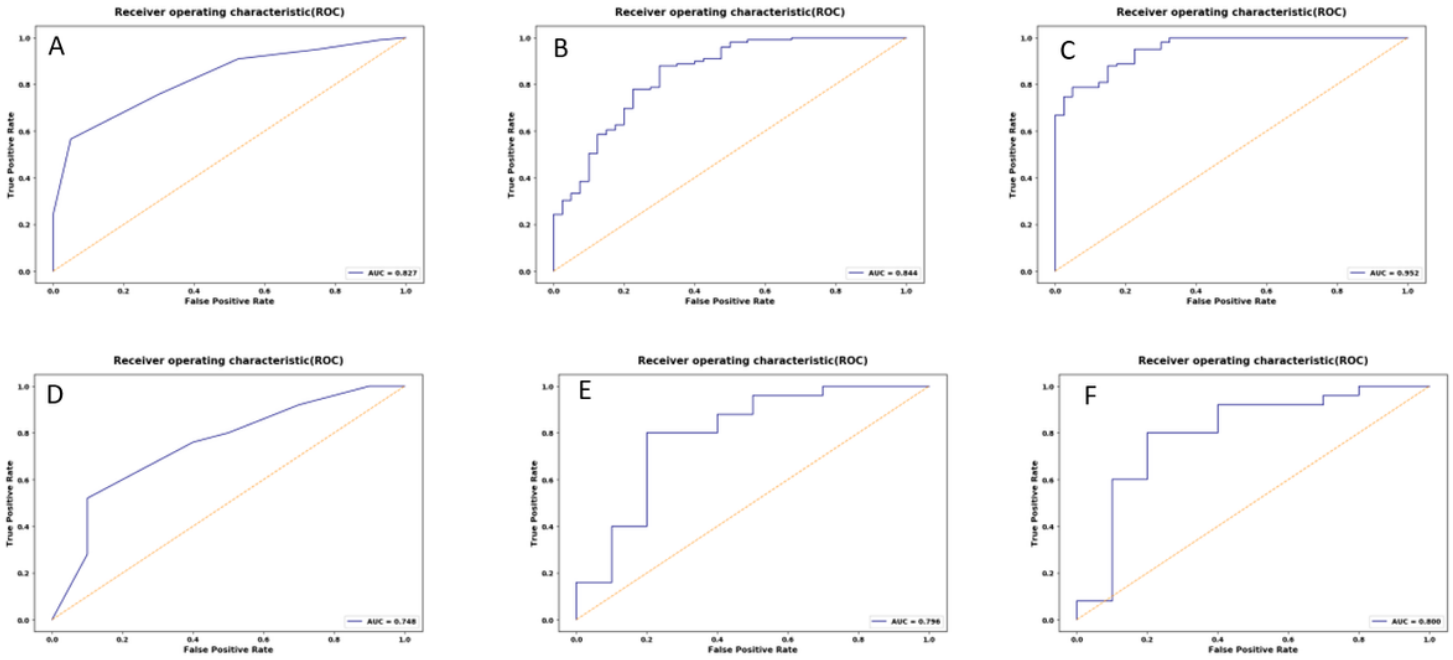

Figure 4

ROC curves of the KNN(A), LR(B), MLP(C) classifiers in the training set. ROC curves of the KNN(D), LR(E), MLP(F)classifiers in the test set.

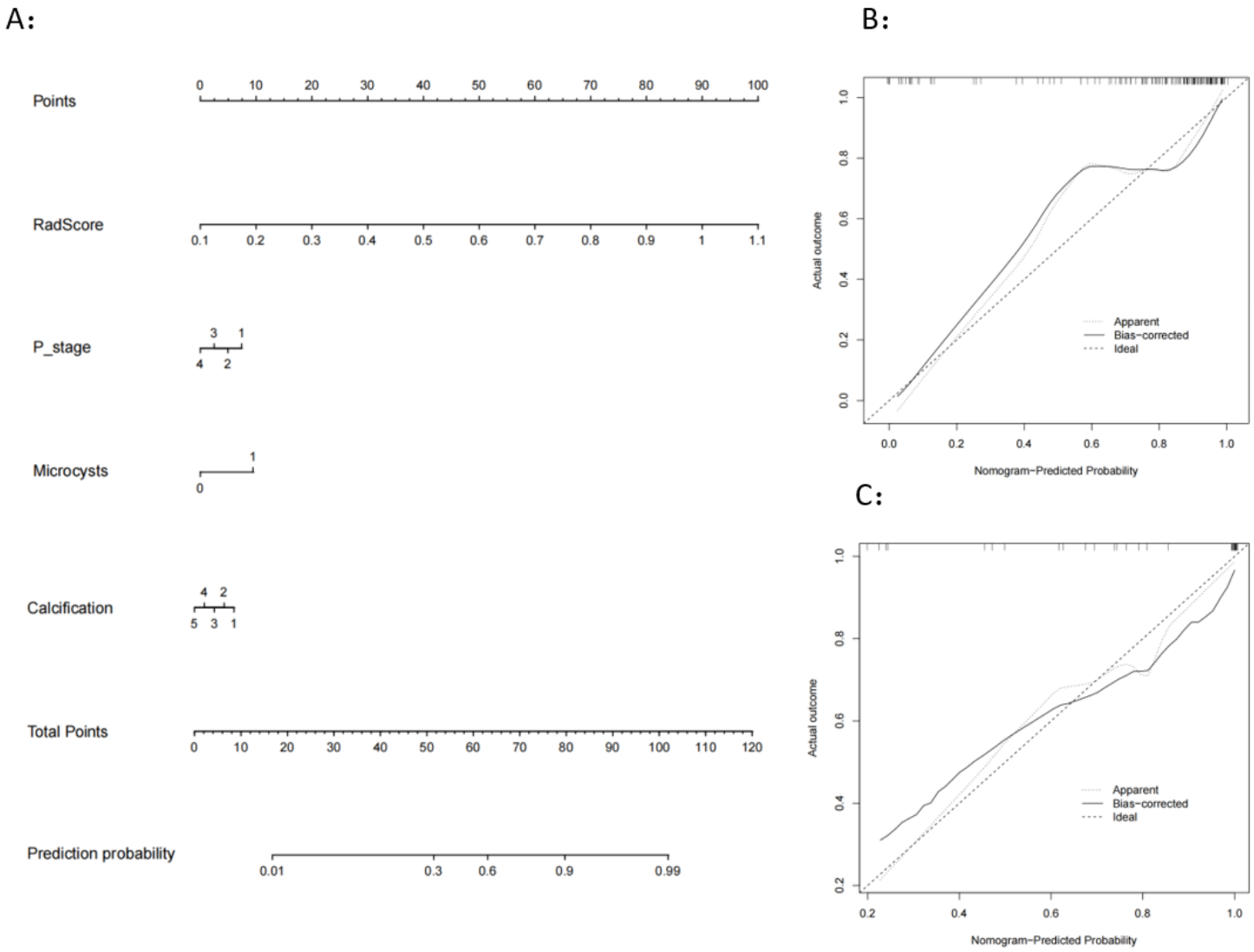

Figure 5

A: The nomogram to predict the biological activity of HAE. The nomogram was developed in the training set with radiomics signature and HAE related clinical indicators. ; B: Calibration curve for training dataset; C: Calibration curve for test dataset.

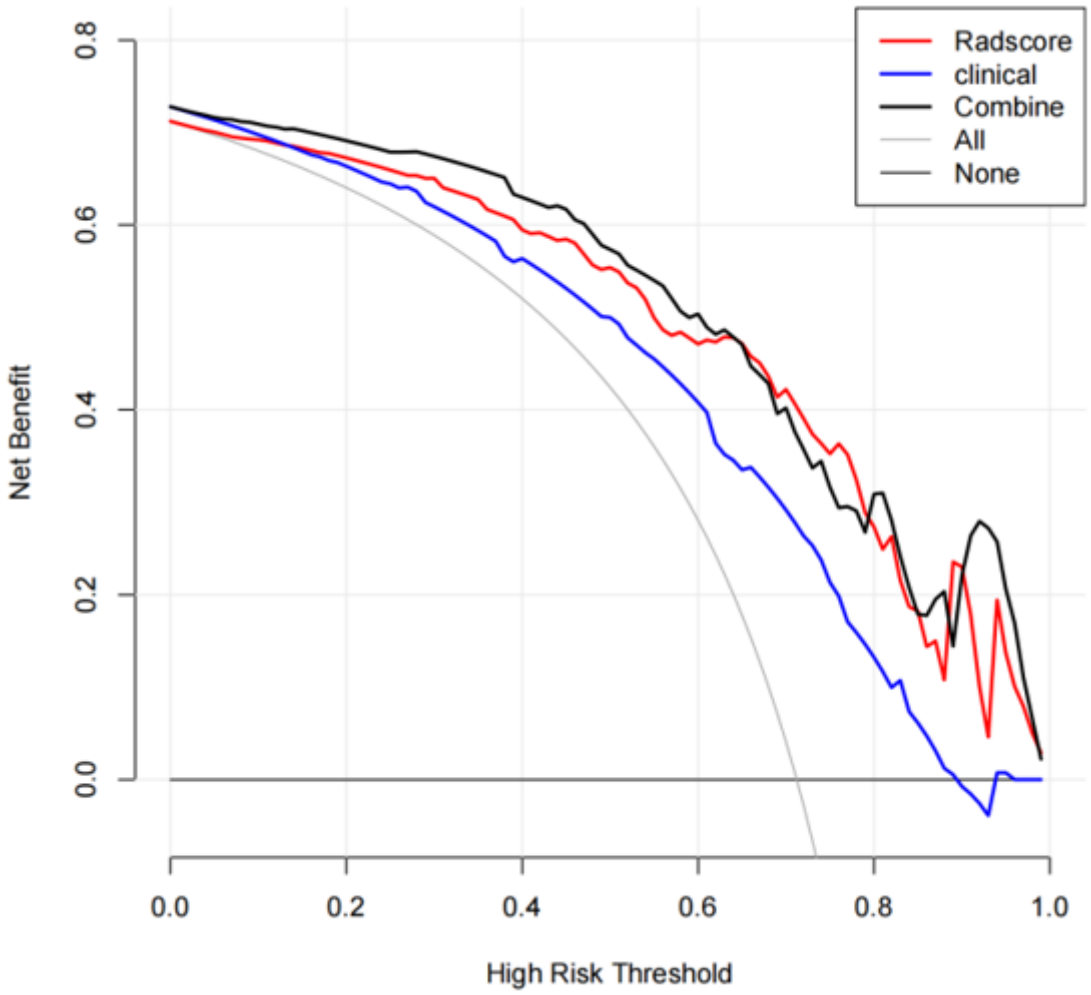

Figure 6

Decision curve for models. Y-axis represents the net benefit, which is calculated by gaining true positives and deleting false positives. The X-axis is the probability threshold.

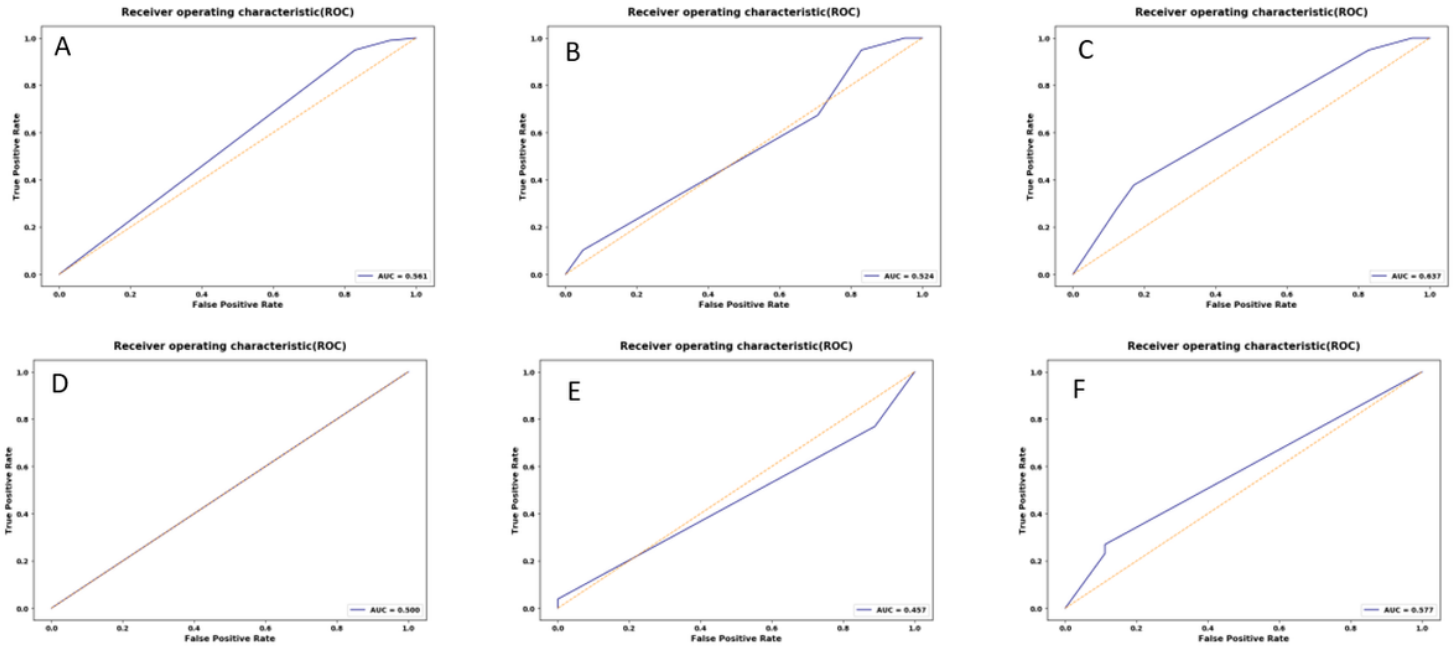

Figure 7

The ROC for Graeter classification based models KNN(A), LR(B), MLP(C) in the training set and KNN(D), LR(E), MLP(F) in the test set.

Supplementary Files

This is a list of supplementary files associated with this preprint. Click to download.

- GraphicalAbstract.pptx
- renamed2bc11.docx
- renamed873de.docx